CHEMISTRY OF MATERIALS

ARTICLE

pubs.acs.org/cm

Graphene Nanosheet/Ni^{2+}/Al^{3+} Layered Double-Hydroxide Composite as a Novel Electrode for a Supercapacitor

Zan Gao,[†] Jun Wang,*[,†,‡] Zhanshuang Li,[†] Wanlu Yang,[†] Bin Wang,[†] Mengjie Hou,[†] Yang He,[†] Qi Liu,[†] Tom Mann,[†] Piaoping Yang,[†,‡] Milin Zhang,[†,‡] and Lianhe Liu[†,‡]

[†]Key Laboratory of Superlight Material and Surface Technology, Ministry of Education, and [‡]Institute of Advanced Marine Materials, Harbin Engineering University, 150001 People's Republic of China

ABSTRACT: A hybrid chemically converted graphene nanosheet/Ni^{2+}/Al^{3+} layered double-hydroxide (GNS/LDH) composite for supercapacitor material has been fabricated by a hydrothermal method. Scanning electron microscopy and transmission electron microscopy results reveal that Ni^{2+}/Al^{3+} LDH platelets homogeneously grew onto the surfaces of the GNSs as spacers to keep the neighboring sheets separate. Electrochemical properties were characterized by cyclic voltammetry, galvanostatic charge/discharge measurements, and electrochemical impedance spectroscopy. The composite exhibits a maximum specific capacitance of 781.5 F/g and excellent cycle life with an increase of the specific capacitance of 38.07% after 50 cycle tests. Even after 200 cycle tests, the increase of the capacitance is 22.56% compared with the initial capacitance.

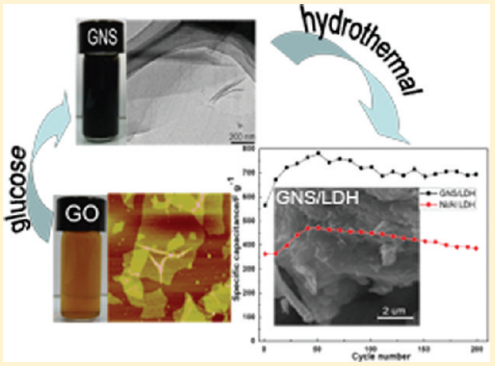

KEYWORDS: graphene nanosheet, layered double hydroxides, composite electrode, supercapacitor

1. INTRODUCTION

Energy is one of the most important topics in the 21st century. The rapid depletion of fossil fuels and deteriorating environmental pollution call for not only renewable and clean energy sources but also more advanced energy storage and management devices.[1] Supercapacitors (SCs), known as electrochemical supercapacitors (ESCs) or ultracapacitors, are considered as promising candidates for energy storage due to their high-power performance, long cycle life, and low maintenance cost.[2,3] Due to higher power capability and relatively larger energy density compared with conventional capacitors, supercapacitors offer a promising potential to meet the increasing power demands of energy storage systems. Thus, supercapacitors show potential applications in communication, transportation, electronics, and aviation.[4]

Supercapacitors can be categorized into two main types on the basis of their charge-storage mechanisms: (i) electrical double-layer capacitors (EDLCs), where the electrical charge is stored at the interface between the electrode and the electrolyte; (ii) redox electrochemical capacitors, where capacitance arises from reversible faradic reactions taking place at the electrode/electrolyte interface. To date, carbon-based materials (activated carbons, carbon aerogels, carbon nanotubes, carbon fabrics, and reduced graphene oxide),[5−10] transition-metal oxides and hydroxides (RuO_2,[11] MnO_2,[12] Co_3O_4,[13] NiO,[14] $Ni(OH)_2$),[15] and conducting polymers (polyaniline, polypyrrole, and polythiophene)[16−19] have been extensively employed as the most promising materials for supercapacitors. However, each material has its unique advantages and disadvantages for SC application. For example, carbon material has high power density and long life cycle, but the small double-layer capacitance limits its application. Transition-metal oxides, hydroxides, and conducting polymers (polyaniline) have been widely investigated due to their relatively higher capacitance and fast redox kinetics, while the relatively low mechanical stability and cycle life are major limitations for SCs. During the past decade, considerable efforts have been exerted to couple the unique advantages of these capacitive materials for SCs.[15,20,21]

Recently, two-dimensional graphene has attracted a great deal of attention due to its high surface area, electrical conductivity, high flexibility, and mechanical strength[22−24] and exhibits great promise for potential applications in the fields of nanoelectronics, sensors, batteries, supercapacitors, hydrogen storage, and nanocomposites.[25] Especially, graphene-based supercapacitors have been reported with a specific capacitance from 117 to 205 F/g in aqueous solution.[26−28] However, the observed capacitances are mainly limited by the agglomeration of graphene sheets and thus cannot reflect the intrinsic capacitance of an individual graphene sheet. Recently, to exploit the potential of graphene-based materials for supercapacitors, one promising prospective is to utilize this ideal single-atom-thick graphene nanosheet (GNS) as a substrate for growth of functional nanomaterials to form new nanocomposites.[29,30] Some kinds of graphene composites, such as GNS/MnO_2,[31] GNS/ZnO and GNS/SnO_2,[32] and GNS/polyaniline,[33] have been prepared for supercapacitors in an aqueous electrolyte. The anchored

Received: April 6, 2011
Revised: June 21, 2011
Published: July 07, 2011

nanoparticles improve the electrochemical performance of graphene-based supercapacitors, as they can contribute pseudocapacitance to the total capacitance apart from the double-layer capacitance from graphene sheets.

Layered double hydroxides (LDHs) are well-known anionic or hydrotalcite-like clays with the general chemical formula $[M^{II}_{1-x}M^{III}_{x}(OH)_2]^{x+}[A^{n-}]_{x/n}\cdot mH_2O$, where M^{II} and M^{III} are divalent and trivalent cations and A^{n-} can be almost any organic or inorganic anion.[34] Due to their anion exchange property and capacity to intercalate anions, LDH materials have been widely employed in catalysts,[35] anion exchangers,[36] precursors to oxides,[37] magnetics,[38] and electrodes for alkaline secondary batteries.[39] Recently, LDH materials containing transition metals have been reported to be promising electrode materials for supercapacitors because of their relatively low cost, high redox activity, and environmentally friendly nature.[40−42] Wang et al. studied the electrochemical properties of double oxides obtained from the annealing of Co/Al LDH, which has a specific capacitance of 684 F/g at a current density of 60 $mA\cdot g^{-1}$.[43] In our previous report, the electrodes of Ni/Al LDH coated on the surface of nickel foam display a specific capacitance of 701 F/g at a current density of 10 $mA\cdot cm^{-2}$.[44] However, up to now, no work on the GNS/LDH composite as electrode material for supercapacitors has been reported.

Herein, we report a simple and green method to fabricate a hybrid GNS/LDH material under mild hydrothermal conditions. In the synthetic procedure, the exfoliated graphite oxide (GO) is reduced to graphene using glucose as the reductant, and then Ni/Al LDH platelets are formed in situ on the surfaces of the GNSs. The reductant and the oxidized product used in this method are environmentally friendly, and the Ni/Al LDH platelets homogeneously anchor onto graphene sheets, which can be spacers to keep neighboring sheets separate. The graphene sheets overlap with each other to afford a three-dimensional conducting network, which facilitates fast electron transfer between the active materials and the charge collector and thus improves the contact between the electrode materials and the electrolyte. The as-obtained GNS/LDH composite exhibited a high specific capacitance (781.5 F/g at 5 $mV\cdot s^{-1}$) and excellent long cycle life. Furthermore, the effect of the microstructure on the electrochemical performance of the composite has also been investigated.

2. EXPERIMENTAL SECTION

2.1. Synthesis of the GNS/LDH Composite. All the chemicals are of analytical grade and were used without further purification. Graphite oxide was prepared from natural graphite by a modified Hummers method.[45] Exfoliation of GO was achieved by ultrasonication of the dispersion on an ultrasonic bath (KQ-500DB, 250 W). Compared with the traditional procedure using highly toxic hydrazine as the reductant, glucose was used as the reducing agent to prepare the GNS.[46] Typically, 2 g of glucose was added to 250 mL of homogeneous GO dispersion (0.5 mg/mL), followed by stirring for 30 min. Then 1 mL of aqueous ammonia solution (25%, w/w) was added to the resulting dispersion. After being vigorously shaken for a few minutes, the mixture was stirred for 60 min at 95 °C. The resulting black dispersion was then filtered and washed with distilled water several times, and the obtained GNS was redispersed in water for further use.

The GNS/LDH composites were synthesized via an in situ crystallization technique. Briefly, 250 mL of the as-obtained GNS suspension (0.5 mg/mL) was transferred into an autoclave pressure vessel, and then certain amounts of $Ni(NO_3)_2\cdot 6H_2O$, $Al(NO_3)_3\cdot 9H_2O$, and urea (0.727, 0.479, and 0.526 g, respectively) were added to the above GNS suspension. Then the mixture was kept at 95 °C for 24 h. Finally, the composites were filtered, washed several times with distilled water and alcohol, and dried at 80 °C for 12 h in a vacuum oven. For comparison, pure Ni/Al LDH was prepared under the same conditions except for the GNS.

2.2. Characterization Methods. The crystallographic structures of the materials were determined by a powder X-ray diffraction (XRD) system (Rigaku TTR-III) equipped with Cu Kα radiation (λ = 0.15406 nm). X-ray photoelectron spectroscopy (XPS) measurements were performed using a PHI 5700 ESCA spectrometer with monochromated Al Kα radiation ($h\nu$ = 1486.6 eV). All XPS spectra were corrected by the C1s line at 284.5 eV. Raman measurements were carried out using a Jobin Yvon HR800 micro-Raman spectrometer at 457.9 nm. The laser beam was focused with a 50× objective lens to an about 1 lm spot on the surface of the sample. The microstructure of the samples was investigated by atomic force microscopy (AFM; Nanoscope IIIa), scanning electron microscopy (SEM; JEOL JSM-6480A microscope), and transmission electron microscopy (TEM; Philips CM 200 FEG, 160 kV). Surface area measurements were carried out by physical adsorption of N_2 at 77 K (Micromeritics ASAP 2010) and obtained by the Brunauer−Emmett−Teller (BET) method.

2.3. Preparation of Electrodes and Electrochemical Characterization. The working electrodes was fabricated by a reported procedure.[47,48] Briefly, the as-prepared materials, acetylene black, and poly(tetrafluoroethylene) (PTFE) were mixed in a mass ratio of 80:15:5 and dispersed in ethanol to produce a homogeneous paste. Acetylene black and PTFE were used as the conductive agent and binder, respectively. Then the resulting mixture was coated onto the nickel foam substrate (1 cm ×1 cm) with a spatula. Finally, the fabricated electrodes were dried at 60 °C for 8 h in a vacuum oven.

The electrochemical properties of the as-obtained products were investigated under a three-electrode electrochemical cell. The Ni foam coated with the GNS/LDH composite was used as the working electrode, and platinum foil (1 cm × 1 cm) and a saturated calomel electrode (SCE) were used as the counter and reference electrodes, respectively. The measurements were carried out in 6 M KOH aqueous electrolyte at room temperature. Cyclic voltammograms, galvanostatic charge/discharge curves, and electrochemical impedance spectroscopy (EIS) were measured by a CHI 660D electrochemical workstation. Cyclic voltammetry (CV) tests were done between 0 and 0.6 V (vs SCE) at scan rates of 5, 10, 20, and 50 $mV\cdot s^{-1}$. Galvanostatic charge/discharge curves were measured in the potential range of 0−0.47 V (vs SCE) at different current densities, and EIS measurements were also carried out in the frequency range from 100 kHz to 0.05 Hz at open circuit potential with an ac perturbation of 5 mV.

3. RESULTS AND DISCUSSION

3.1. Material Characterization. XRD patterns of GO, GNS, Ni/Al LDH, and the hybrid GNS/LDH material are shown in Figure 1. The diffraction peak of exfoliated GO at 10.8° (001) features a basal spacing of 0.82 nm, showing the complete oxidation of graphite to the graphite oxide due to the introduction of oxygen-containing functional groups on the graphite sheets (Figure 1a).[49] After GO is reduced to a GNS by glucose, most of the oxygen-containing groups are removed. For the XRD pattern of the GNS (Figure 1b), the peak located at 10.8° disappears, while a broad diffraction peak (002) appears at a 2θ of about 24.5°, revealing the great reduction of GO and the exfoliation of the layered GNS.[50,51] The interlayer spacing of the GNS changes from 0.8 nm for GO to 0.37 nm, which is still a little

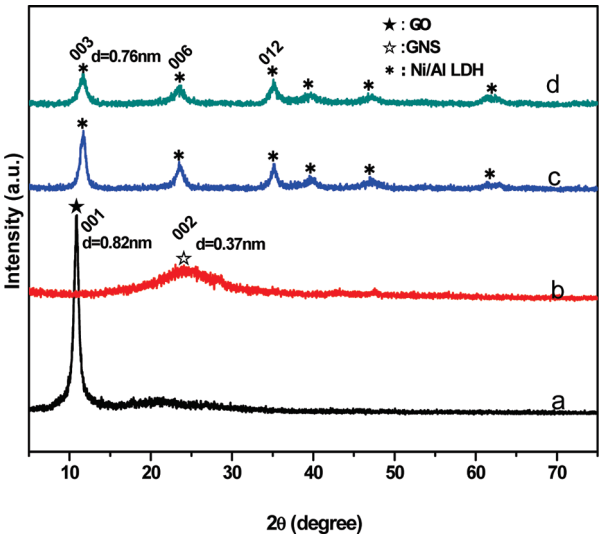

Figure 1. Typical XRD patterns of GO (a), the GNS (b), Ni/Al LDH (c), and the prepared GNS/LDH composite (d).

larger than that of natural graphite (0.34 nm). This can be interpreted by the $\pi-\pi$ stacking interaction between the graphene sheets leading to the formation of the agglomerates. However, the residual oxygen functionalities on the reduced GO surfaces induce electrostatic repulsion, stabilizing the graphene sheets. These residual oxygenated functional groups most likely involve the intercalation and adsorption of metal ions onto the GNS. The XRD patterns of the as-prepared pure Ni/Al LDH and hybrid GNS/LDH materials can be indexed to hexagonal Ni/Al LDH (JCPDS no. 22-0452), and no characteristic peak of graphite oxide is observed. For GNS/LDH materials, the (002) peak of the layered GNS has almost disappeared and the *d* spacing of the (003) diffraction peak of Ni/Al LDH is 0.76 nm. The result suggests that the restacking of the graphene sheets is effectively prevented from a complete exfoliation state of graphite in the hybrid GNS/LDH material, corresponding to the TEM image in Figure 5f, showing some thin hexagonal LDH nanoplatelets located on the surfaces of the GNSs. Previous research also shows that if the regular stacks of graphite oxide or graphite are destroyed, the diffraction peaks will become weak or even disappear.[52−54] However, the relatively weaker intensity of the peaks of GNS/LDH than that of pure Ni/Al LDH means a low crystallinity of the hybrid material.

Figure 2a shows the XPS spectra of GO, as-prepared GO, and the GNS/LDH composite. The binding energies in the XPS experiment were corrected by referencing the C1s peak to 284.5 eV. Compared to that of GO, the XPS spectrum of the GNS/LDH composite not only exhibits a relatively low O1s peak and C1s peak, but also exhibits two peaks at 876.7 and 858.8 eV corresponding to $Ni2p_{1/2}$ and $Ni2p_{3/2}$, which also confirm the presence of Ni/Al LDH in the composite. The C1s XPS spectrum of GO (Figure 2b) clearly indicates a considerable degree of oxidation with three components that are assigned to carbon atoms in different functional groups: the nonoxygenated ring C (C−C), the C in C−O bonds (C−O), and the carboxylate carbon (O—C═O).[55,56] The areas of the three C1s components of graphite oxide show that the nonoxygenated ring C is about 43% (284.5 eV), while that of the hybrid GNS/LDH composite is 74%. Results indicate that most of the oxygen

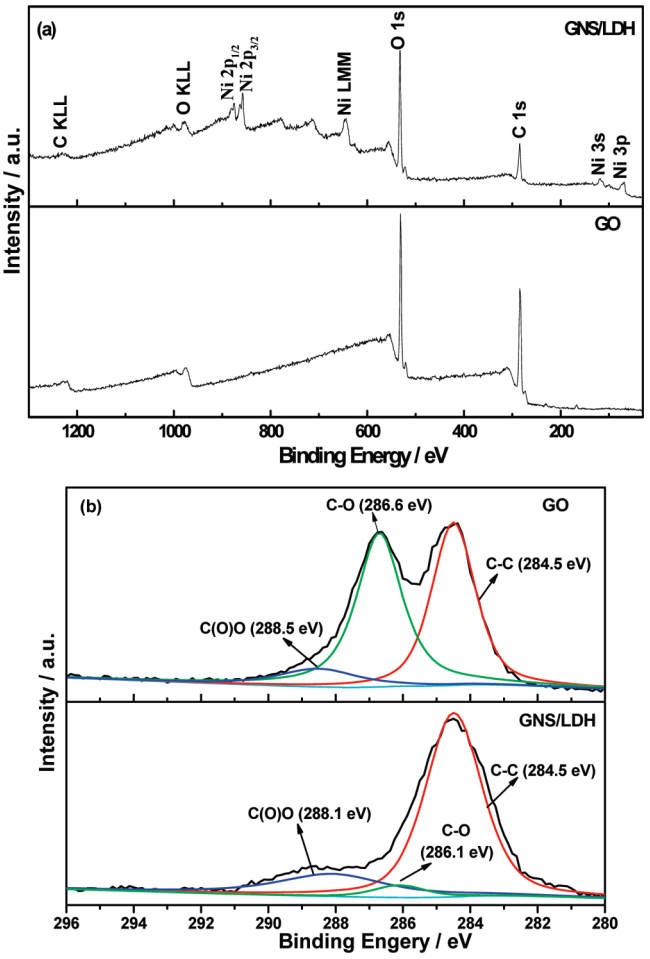

Figure 2. XPS survey spectra (a) and C1s XPS spectra (b) of GO and the GNS/LDH composite.

functional groups in GO are successfully removed. On the other hand, the absorbance band intensities of the carbonyl carbon (C−O) and the carboxylate carbon (O—C═O) decrease sharply for the hybrid GNS/LDH composite due to the reduction of GO to graphene by glucose.

Raman spectroscopy is a nondestructive approach to characterize graphitic materials, in particular to determine ordered and disordered crystal structures of graphene.[57] The Raman spectrum of graphene is usually characterized by two main features: the G band arising from the first order scattering of the E_{1g} phonon of sp^2 C atoms (usually observed at 1575 cm^{-1}) and the D band arising from a breathing mode of point photons of A_{1g} symmetry (1350 cm^{-1}).[58] Figure 3 shows the Raman spectra of GO, the GNS, Ni/Al LDH, and the GNS/LDH composite. A broad D band and a broad G band are observed in the Raman spectra of GO, the GNS, and GNS/LDH. Compared with GO (Figure 3a), an increased I_D/I_G intensity ratio for the GNS (Figure 3b) and GNS/LDH (Figure 3d) is observed, indicating a decrease in the size of the in-plane sp^2 domains[59,60] and the removal of the oxygen functional groups in the graphite oxide sheet, which is consistent with XPS results. In addition, in the Raman spectrum of the GNS/LDH composite (Figure 3d), besides the G band and D band, two broad bands at 575 and 1065 cm^{-1} are apparent, which should be related to the typical Raman peaks of Ni/Al LDH (Figure 3c).

dx.doi.org/10.1021/cm200975x |*Chem. Mater.* 2011, 23, 3509–3516

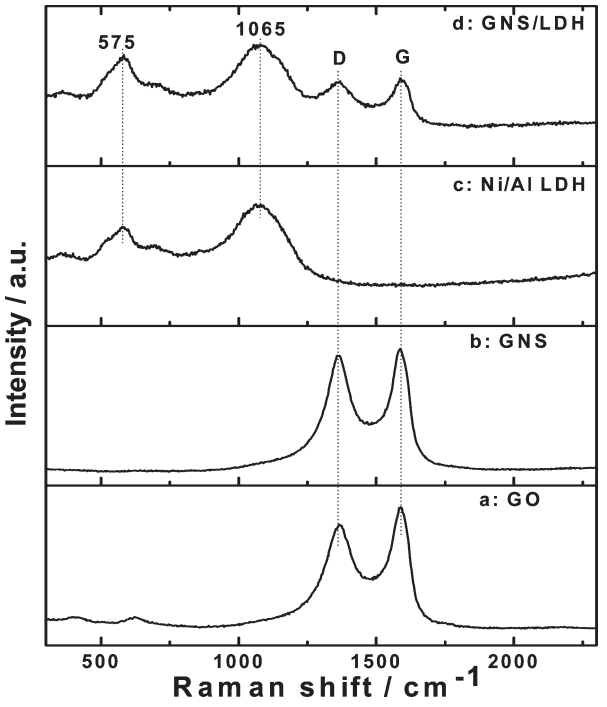

Figure 3. Raman spectra of GO (a), GNS (b), Ni/Al LDH (c) and the GNS/LDH composite (d).

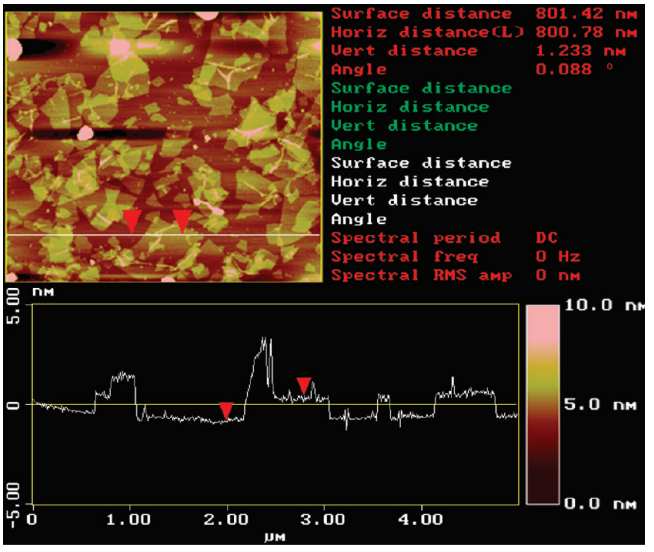

Figure 4. AFM image of exfoliated GO sheets on a mica surface with the height profile.

Figure 4 gives a typical AFM image of an exfoliated GO dispersion in water after deposition on a freshly cleaved mica surface. The average thickness of as-prepared GO measured from the height profile of the AFM image is about 1.2 nm, which corresponds to a single-layer GO.[61] Compared with the theoretical values of 0.78 nm for single-layer graphene, the higher thickness of GO may arise from oxygen-containing groups on the surfaces.[62] This ideal single-atom-thick GNS as a support to anchor functional nanomaterials to form new composites should be highly promising.

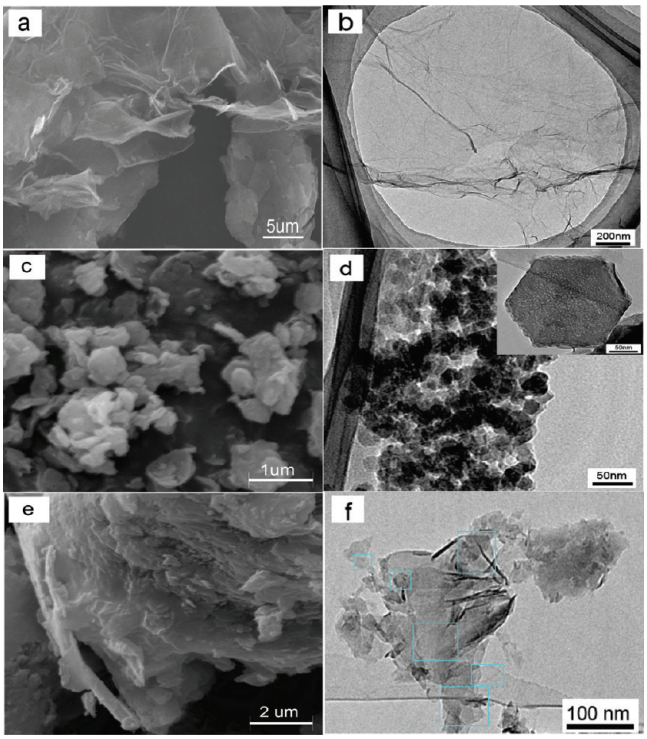

Figure 5. SEM (a) and TEM (b) images of pure GNSs. SEM (c) and TEM (d) images of pure Ni/Al LDH (the inset exhibits the corresponding magnified TEM image). SEM (e) and TEM (f) images of GNS/LDH composites.

The morphology and structure of the as-obtained products are shown in Figure 5. It can be seen that the corrugated and scrolled sheets resemble crumpled silk veil waves (Figure 5a). GNSs agglomerate with each other through van der Waals interactions of the remaining oxygen-containing functionalities (epoxide, hydroxyl, carbonyl, and carboxyl groups) on the surfaces of the GNSs. The TEM images show that the GNS has corrugations and scrollings on the edge of the graphene sheet. From SEM and TEM images (Figure 5c,d), Ni/Al LDH consists of irregular and thin hexagonal platelets with a mean lateral size of 50 nm, while most of the LDH sheets stack with each other to form agglomerates. As for the GNS/LDH composite (Figure 5e,f) after thermal treatment, thin hexagonal LDH platelets decorated on the graphene nanosheets exhibit loose lamellar structures. Because Ni/Al LDH nanoplatelets are distributed on the surfaces of graphene nanosheets, the restacking of graphene nanosheets was effectively prevented, thus avoiding the loss of their highly active surface area. The BET surface areas of the GNS, pure Ni/Al LDH, and the GNS/LDH composite were determined to be 298.65, 28.52, and 87.22 m^2/g, respectively. The graphene sheets overlap with each other to give a three-dimensional conducting network for fast electron transfer between the active materials and the charge collector. This open structure may be favorable for the improvement of the electrochemical performance as an electrode for supercapacitors.

On the basis of the above results, a schematic representation of the formation process for the hybrid GNS/LDH material is given in Figure 6. GO sheets have basal planes covered mostly by epoxy and hydroxyl groups, while carbonyl and carboxyl groups are located at the edges. These functional groups act as anchor sites

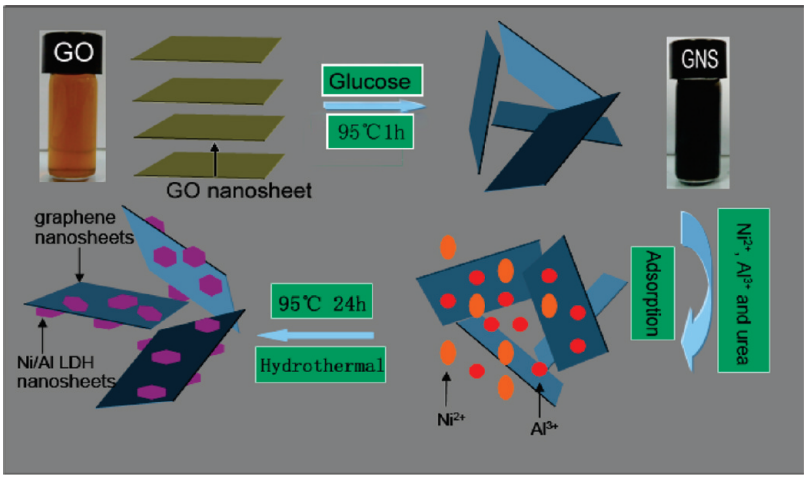

Figure 6. Schematic representation of the formation process of the hybrid GNS/LDH composite.

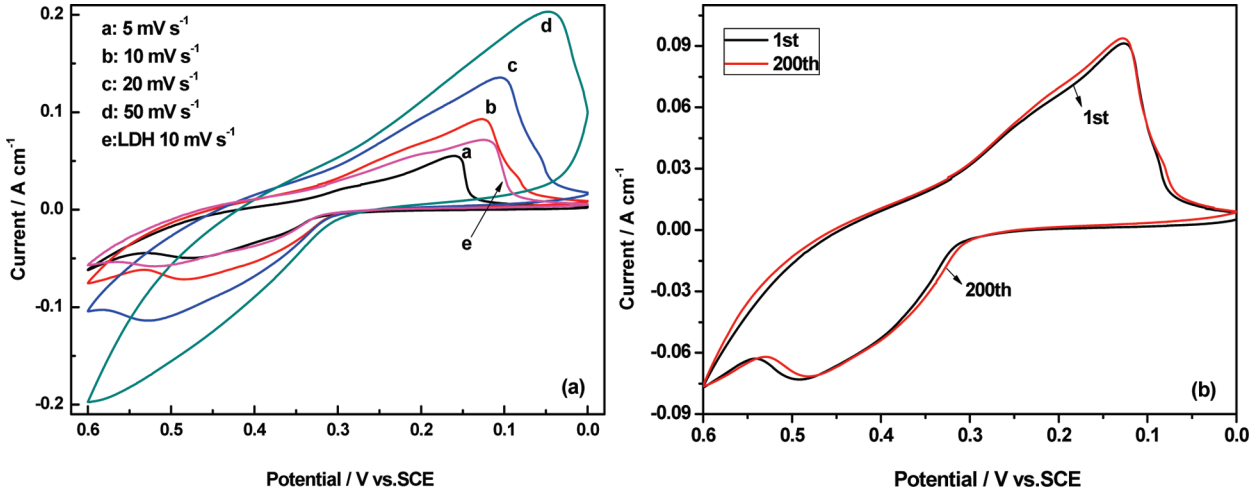

Figure 7. (a) CV curves of the GNS/LDH composite at different scan rates of 5, 10, 20, and 50 mV·s^{-1} in 6.0 M KOH solution. (b) CV curves of the GNS/LDH composite at the 1st and 200th cycles.

and enable the subsequent in situ formation of nanostructures on the surfaces and edges of GO sheets. However, these oxygen-containing functional groups impair the conductivity of GO sheets to such an extent that they are not suitable for electrode materials. After the reduction by glucose, most of the oxygen-containing groups on GO sheets are removed, and the conductivity of the GNS is recovered, which improves the electrochemical property of the GNS/LDH composite.[60] When the as-prepared GNS was soaked in a mixed solution of $Ni(NO_3)_2 \cdot 6H_2O$, $Al(NO_3)_3 \cdot 9H_2O$, and urea, metal ions (Ni^{2+} and Al^{3+}) could be adsorbed onto the surfaces of GO nanosheets due to the electrostatic force between the metal ions and negatively charged residual oxygen-containing functional groups. Finally, Ni/Al LDH platelets grow onto the surfaces of graphene nanosheets under a hydrothermal treatment. The Ni/Al LDH platelets are intercalated into the graphene nanosheets, which effectively prevents their restacking. Consequently, the graphene nanosheets keep their highly active surface area. In addition, the capacity and cyclic performance of graphene-based material are increased to some extent,[63] which is proved in the following test.

3.2. Electrochemical Behavior. To explore the potential application of the as-synthesized GNS/LDH nanocomposite, the samples were fabricated as supercapacitor electrodes and characterized by CV, EIS, and galvanostatic charge/discharge measurements.

Figure 7a shows the cyclic voltammogram of the GNS/LDH composite at scan rates of 5, 10, 20, and 50 mV·s^{-1} in 6 M KOH solution. For each curve, a pair of redox peaks with an anodic peak at around 0.1 V and a cathodic peak at about 0.48 V are observed, which correspond to the conversion between different oxidation states of Ni according to the following equation:[64]

$$Ni(OH)_2 + OH^- \rightarrow NiOOH + H_2O + e^- \quad (1)$$

The potential difference ($\Delta E_{a,c}$) between the anodic and cathodic peaks is used as a measure of the reversibility of the electrochemical redox reaction: the higher the reversibility, the smaller the $\Delta E_{a,c}$.[65] However, at different scans, $\Delta E_{a,c}$ is higher than the theoretical value of 59 mV, which means that the electrode is not reversible,[66] while each curve at different scans keeps similar redox couples, indicating that quasi-reversible

dx.doi.org/10.1021/cm200975x |*Chem. Mater.* 2011, 23, 3509–3516

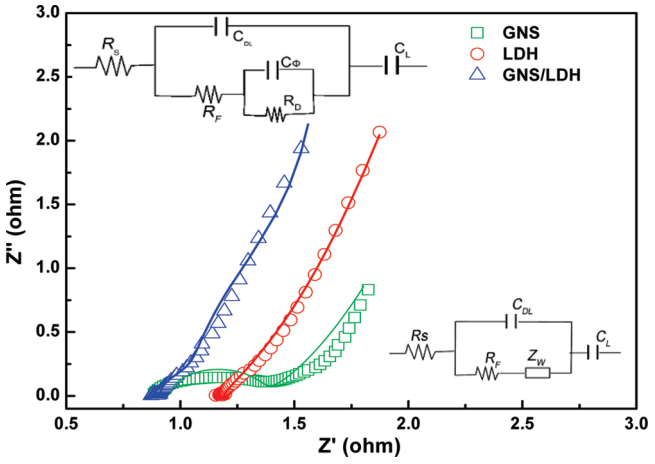

Figure 8. Nyquist plots of experimental impedance data (scattering dot) and fitting results (solid line) for the GNS, pure Ni/Al LDH, and GNS/LDH composite electrodes. The insets show the electrical equivalent circuit used for fitting the impedance spectra (upper left for Ni/Al LDH and GNS/LDH, lower right for the GNS).

and continuous faradic redox reactions of Ni/Al LDH are involved during the charge and discharge processes, which mainly contribute to the pseudocapacitance. The cyclability of the GNS/LDH composite was measured at the 1st and 200th cycles shown in Figure 7b. After 200 cycles, the current response almost remained constant and the peak potential position changed very little, which indicate a good electrochemical reversibility.[67] In addition, the area surrounded by CV curves for the GNS/LDH electrode is apparently larger than that of the pure Ni/Al LDH electrode at the same scan rate (Figure 7a, curves b and e), implying a higher specific capacitance of the GNS/LDH electrode. The results are also consistent with the galvanostatic charge/discharge measurements.

EIS analysis is a principal method to examine the fundamental behavior of electrode materials for supercapacitors. For further understanding, the impedance of the pure GNS, Ni/Al LDH, and the GNS/LDH composite were measured in the frequency range of 100−0.05 kHz at open circuit potential with an ac perturbation of 5 mV (Figure 8). The measured impedance spectra were analyzed using the CNLS fitting method based on the equivalent circuit,[2] which is given in the inset of Figure 8. It is found that the impedance spectrum of the GNS is much different from that of Ni/Al LDH and GNS/LDH, which displays a typical characteristic of carbon materials corresponding to the lower right corner equivalent circuit. R_s is the resistance related to the ionic conductivity of the electrolyte and electronic conductivity of the electrodes and current collectors, C_{DL} is the double-layer capacitance on the grain surface, and R_F in parallel with C_{DL} is mainly associated with the faradic reactions. C_L is the limit capacitance.[68] The slope of the 45° portion of the curve is called the Warburg resistance (Z_W) and is a result of the frequency dependence of ion diffusion/transport in the electrolyte.[27] As a representation of the double-layer capacitance behavior of the GNS, an equivalent circuit was given for the pseudocapacitance (C_φ) behavior of Ni/Al LDH and GNS/LDH (the upper-left representation in Figure 8). The values of R_s, C_{DL}, R_F, R_D, Z_W, and C_L calculated from CNLS fitting of the experimental impedance spectra are presented in Table 1. Obviously, the R_s and R_F of the GNS/LDH composite electrode are smaller

Table 1. Calculated Values of R_s, C_{DL}, R_F, C_φ, R_D, Z_W, and C_L through CNLS Fitting of the Experimental Impedance Spectra Based upon the Proposed Equivalent Circuit in Figure 8

	R_s (Ω)	C_{DL} (F)	R_F (Ω)	C_φ (F)	R_D (Ω)	Z_W (Ω)	C_L (F)
GNS	0.9505	0.0009276	0.3995			1.231	1.496
Ni/Al LDH	1.191	0.3119	0.2966	1.493	0.6162		0.9752
GNS/LDH	0.9044	0.3247	0.2368	1.438	0.5513		1.012

than those of the Ni/Al LDH and pure GNS electrodes, which is probably due to the prevention of the aggregation for graphene sheets by the anchored LDH particles on the GNS. At the same time, the graphene sheets overlap each other to form a conductive network through sheet plane contact, which facilitates the fast electron transfer between the active materials and the charge collector. This structure improves the electrochemical performance of the composite electrode, showing a synergistic effect of Ni/Al LDH and the GNS.

The galvanostatic charge/discharge measurement was performed to calculate the specific capacitance of the electrode according to the following equation:

$$C_{sp} = \frac{it}{(\Delta v)m} \qquad (2)$$

where i, t, Δv, and m are the constant current (A), discharge time (s), total potential deviation (V), and mass of active materials (g), respectively.

Figure 9 shows charge/discharge curves of the Ni/Al LDH and GNS/LDH composite electrodes in 6.0 M KOH solution at different galvanostatic current densities. Figure 9A shows the first charge/discharge curves of the Ni/Al LDH and GNS/LDH electrodes in 6.0 M KOH solution at a galvanostatic current density of 5 mA·cm^{-2}, it can be seen that both of the discharge curves consist of two clear voltage stages: a fast potential drop (from 0.45 to 0.35 V) and a slow potential decay (from 0.35 to 0.2 V). The former results from internal resistance, and the latter represents the pseudocapacitive feature of the electrode. There is obvious deviation of the discharge curves from a straight line, which demonstrates that the capacitance mainly comes from the faradic redox reaction of Ni species in Ni/Al LDH. The discharge time of the GNS/LDH composite is longer than that of Ni/Al LDH powder at the same current density and mass of active materials. Figure 9B shows the galvanostatic charge/discharge tests of the GNS/LDH composite within the potential window of 0−0.47 V (vs SCE) at a current density of 10 mA·cm^{-2}. Each charge/discharge cycle approximately has a potential−time response behavior, which also implies that the charge/discharge process of the GNS/LDH composite electrode is reversible. The first discharge specific capacitances of the Ni/Al LDH and GNS/LDH composite electrodes are 565.87 and 361.97 F/g, respectively (calculated from eq 2), which indicates that the specific capacitance of the hybrid material is remarkably enhanced compared with the corresponding pure Ni/Al LDH. The larger capacitance for GNS/LDH may be caused by the combination of electric double-layer capacitance and faradic pseudocapacitance. At the same time, the open structure system of GNS/LDH improves the contact between the electrode materials and the electrolyte and thus makes full use of the electrochemical active material contribution to the overall capacitance.

dx.doi.org/10.1021/cm200975x |*Chem. Mater.* 2011, 23, 3509–3516

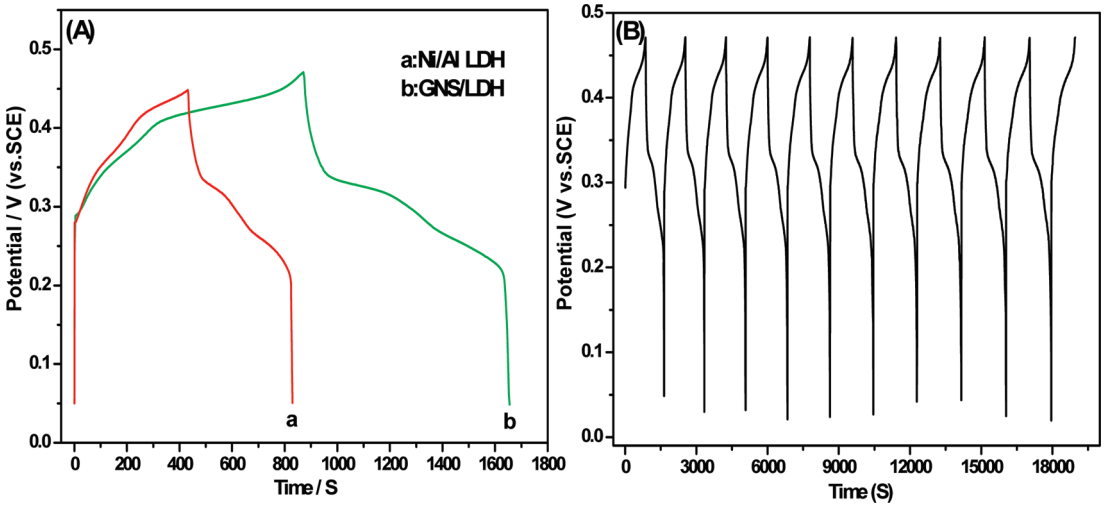

Figure 9. (A) First charge/discharge curves of the Ni/Al LDH electrode (a) and GNS/LDH composite electrode (b) in 6.0 M KOH solution at a galvanostatic current density of 5 mA·cm^{-2}. (B) Galvanostatic charge/discharge tests of the GNS/LDH composite within the potential window of 0−0.47 V (vs SCE) at a current density of 10 mA·cm^{-2}.

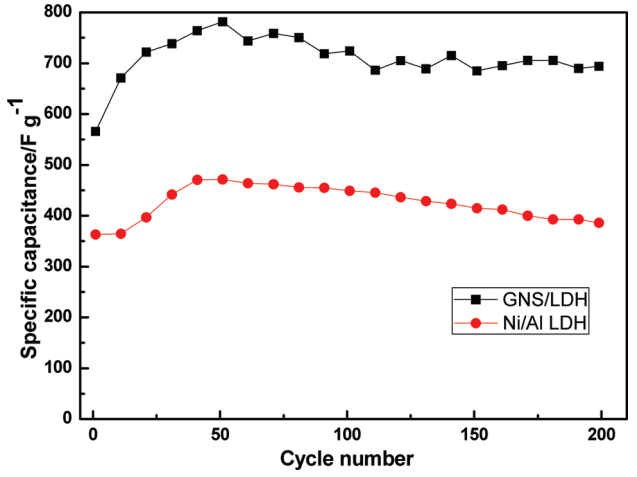

Figure 10. Cyclic performance of pure Ni/Al LDH and GNS/LDH composite electrodes. The charge/discharge tests were performed at 10 mA·cm^{-2} in 6.0 M KOH solution.

The long cycle life of supercapacitors is a crucial parameter for their practical application.[2] Figure 10 shows the cyclic performances of the electrodes examined by galvanostatic charge/discharge tests for 200 cycles. The GNS/LDH composite electrode exhibits a higher specific capacitance and more stable electrochemical performance than the pure Ni/Al LDH electrode over the entire cycle numbers. Interestingly, the specific capacitance of the GNS/LDH composite increases by 38.07% after 50 cycle tests (from 565.87 to 781.5 F/g). Even after 200 cycle tests, the final capacitance (693.7 F/g) still increases by 22.56% from the initial capacitance (566.87 F/g). However, for pure Ni/Al LDH, the initial capacitance, maximum capacitance, and final capacitance after 200 cycle tests are 362.0, 471.6, and 385.8 F/g, respectively, which are lower than those of GNS/LDH. The initial increase of capacitance can be explained as follows: At the initial stage, active materials have not been fully used. After repetitive charge/discharge cycling, the electrochemically active Ni sites inside the nickel foam electrode will be fully exposed to the electrolyte. Therefore, a maximum capacitance was displayed in the cyclic tests. The excellent cycle stability and higher specific capacitance of GNS/LDH may be the reason that the flexible GNSs in composites can not only form an open structure to improve the connection between the active material and electrolyte and make full use of electrochemically active Ni/Al LDH during charge and discharge processes, but also provide the high electrical conductivity of the overall electrode due to the high conductivity of graphene.

4. CONCLUSION

In summary, the GNS/LDH composite as an electrode for supercapacitors was prepared by a hydrothermal method. The surface morphology, structure, and capacitive behaviors of the GNS/LDH composite were well investigated. The incorporation of Ni/Al LDH platelets onto graphene can prevent the restacking of graphene sheets and improve the capacitance of the composite electrode, the electrolyte/electrode accessibility and the conductivity. The prepared GNS/LDH composite exhibited a high specific capacitance (781.5 F/g at 5 mV·s^{-1}) and excellent long cycle life, suggesting its high promising prospective for SCs.

AUTHOR INFORMATION

Corresponding Author

*Phone: +86 451 8253 3026. Fax: +86 451 8253 3026. E-mail: zhqw1888@sohu.com.

ACKNOWLEDGMENT

This work was supported by the Fundamental Research Funds of the Central University (Grant HEUCF101010), Science and Technology Planning Project from the Education Department of Heilongjiang Province (Grant 11553044), High Education Doctoral Fund (Grant 160100110010), and Special Innovation Talents of Harbin Science and Technology (Grant RC2011QN018009).

REFERENCES

(1) Liu, C.; Li, F.; Ma, L. P.; Cheng, H. M. *Adv. Mater.* **2010**, *22*, E28.
(2) Conway, B.E. Electrochemical Supercapacitors. *Scientific Fundamentals and Technological Applications*; Kluwer Academic Publishers, Plenum Press: New York, 1999.
(3) Burke, A. *J. Power Sources* **2000**, *91*, 37.
(4) Kötz, R.; Carlen, M. *Electrochim. Acta* **2000**, *45*, 2483.
(5) Frackowiak, E.; Béguin, F. *Carbon* **2001**, *39*, 937.
(6) Pröbstle, H.; Schmitt, C.; Fricke, J. *J. Power Sources* **2002**, *105*, 189.
(7) Park, J. H.; Ko, J. M.; Park, O. O. *J. Electrochem. Soc.* **2003**, *150*, A864.
(8) Pan, H.; Poh, C. K.; Feng, Y. P.; Lin, J. *Chem. Mater.* **2007**, *19*, 6120.
(9) Murali, S.; Dreyer, D. R.; Valle-Vigon, P.; Stoller, M. D.; Zhu, Y.; Morales, C.; Fuertes, A. B.; Bielawski, C. W.; Ruoff, R. S. *Phys. Chem. Chem. Phys.* **2011**, *13*, 2652.
(10) Kim, T. Y.; Lee, H. W.; Stoller, M.; Dreyer, D. R.; Bielawski, C. W.; Ruoff, R. S.; Suh, K. S. *ACS Nano* **2010**, *5*, 436.
(11) Susanti, D.; Tsai, D. S.; Huang, Y. S.; Korotcov, A.; Chung, W. H. *J. Phys. Chem. C* **2007**, *111*, 9530.
(12) Subramanian, V.; Zhu, H.; Wei, B. *J. Power Sources* **2006**, *159*, 361.
(13) Xu, J.; Gao, L.; Cao, J.; Wang, W.; Chen, Z. *Electrochim. Acta* **2010**, *56*, 732.
(14) Zhao, B.; Ke, X. K.; Bao, J. H.; Wang, C. L.; Dong, L.; Chen, Y. W.; Chen, H. L. *J. Phys. Chem. C* **2009**, *113*, 14440.
(15) Wang, H.; Casalongue, H. S.; Liang, Y.; Dai, H. *J. Am. Chem. Soc.* **2010**, *132*, 7472.
(16) Wang, K.; Huang, J.; Wei, Z. *J. Phys. Chem. C* **2010**, *114*, 8062.
(17) Guan, H.; Fan, L. Z.; Zhang, H.; Qu, X. *Electrochim. Acta* **2010**, *56*, 964.
(18) Biswas, S.; Drzal, L. T. *Chem. Mater.* **2010**, *22*, 5667.
(19) Fan, L. Z.; Hu, Y. S.; Maier, J.; Adelhelm, P.; Smarsly, B.; Antonietti, M. *Adv. Funct. Mater.* **2007**, *17*, 3083.
(20) Zheng, H.; Tang, F.; Jia, Y.; Wang, L.; Chen, Y.; Lim, M.; Zhang, L.; Lu, G. *Carbon* **2009**, *47*, 1534.
(21) Wang, D. W.; Li, F.; Zhao, J.; Ren, W.; Chen, Z. G.; Tan, J.; Wu, Z. S.; Gentle, I.; Lu, G. Q.; Cheng, H. M. *ACS Nano* **2009**, *3*, 1745.
(22) Novoselov, K. S.; Geim, A. K.; Morozov, S. V.; Jiang, D.; Zhang, Y.; Dubonos, S. V.; Grigorieva, I. V.; Firsov, A. A. *Science* **2004**, *306*, 666.
(23) Novoselov, K. S.; Jiang, D.; Schedin., F. *Proc. Natl. Acad. Sci. U.S.A.* **2005**, *102*, 10451.
(24) Dreyer, D. R.; Ruoff, R. S.; Bielawski, C. W. *Angew. Chem., Int. Ed.* **2010**, *49*, 9336.
(25) Yan, J.; Wei, T.; Qiao, W.; Shao, B.; Zhao, Q.; Zhang, L.; Fan, Z. *Electrochim. Acta* **2010**, *55*, 6973.
(26) Vivekchand, S.; Rout, C. S.; Subrahmanyam, K.; Govindaraj, A.; Rao., C. N. R. *J. Chem. Sci.* **2008**, *120*, 9.
(27) Stoller, M. D.; Park, S.; Zhu, Y.; An, J.; Ruoff, R. S. *Nano Lett.* **2008**, *8*, 3498.
(28) Wang, Y.; Shi, Z.; Huang, Y.; Ma, Y.; Wang, C.; Chen, M.; Chen, Y. *J. Phys. Chem. C* **2009**, *113*, 13103.
(29) Kamat, P. V. *J. Phys. Chem. Lett.* **2010**, *1*, 520.
(30) Potts, J. R.; Dreyer, D. R.; Bielawski, C. W.; Ruoff, R. S. *Polymer* **2011**, *52*, 5.
(31) Wu, Z. S.; Ren, W.; Wang, D. W.; Li, F.; Liu, B.; Cheng, H. M. *ACS Nano* **2010**, *4*, 5835.
(32) Lu, T.; Zhang, Y.; Li, H.; Pan, L.; Li, Y.; Sun, Z. *Electrochim. Acta* **2010**, *55*, 4170.
(33) Wu, Q.; Xu, Y.; Yao, Z.; Liu, A.; Shi, G. *ACS Nano* **2010**, *4*, 1963.
(34) Valente, J. S.; Sánchez-Cantú, M.; Lima, E.; Figueras, F. *Chem. Mater.* **2009**, *21*, 5809.
(35) Climent, M. J.; Corma, A.; Iborra, S. *Chem. Rev.* **2010**, *111*, 1072.
(36) Prasanna, S. V.; Kamath, P. V.; Shivakumara, C. *Mater. Res. Bull.* **2007**, *42*, 1028.
(37) Tichit, D.; Ortiz, M. d. J. M.; Francová, D.; Gérardin, C.; Coq, B.; Durand, R.; Prinetto, F.; Ghiotti, G. *Appl. Catal., A* **2007**, *318*, 170.
(38) Taibi, M.; Ammar, S.; Jouini, N.; Fievet, F.; Molinie, P.; Drillon, M. *J. Mater. Chem.* **2002**, *12*, 3238.
(39) Kamath, P. V.; Annal Therese, G. H.; Gopalakrishnan, J. *J. Solid State Chem.* **1997**, *128*, 38.
(40) Béléké, A. B.; Mizuhata, M. *J. Power Sources* **2010**, *195*, 7669.
(41) Wang, Y. G.; Cheng, L.; Xia, Y. Y. *J. Power Sources* **2006**, *153*, 191.
(42) Liu, X. M.; Zhang, Y. H.; Zhang, X. G.; Fu, S. Y. *Electrochim. Acta* **2004**, *49*, 3137.
(43) Wang, Y.; Yang, W.; Zhang, S.; Evans, D. G.; Duan, X. *J. Electrochem. Soc.* **2005**, *152*, A2130.
(44) Wang, J.; Song, Y.; Li, Z.; Liu, Q.; Zhou, J.; Jing, X.; Zhang, M.; Jiang, Z. *Energy Fuels* **2010**, *24*, 6463.
(45) Hummers, W. S.; Offeman, R. E. *J. Am. Chem. Soc.* **1958**, *80*, 1339.
(46) Zhu, C.; Guo, S.; Fang, Y.; Dong, S. *ACS Nano* **2010**, *4*, 2429.
(47) Chen, S.; Zhu, J.; Wu, X.; Han, Q.; Wang, X. *ACS Nano* **2010**, *4*, 2822.
(48) Zhao, X.; Wang, A.; Yan, J.; Sun, G.; Sun, L.; Zhang, T. *Chem. Mater.* **2010**, *22*, 5463–5473.
(49) Liu, Z. h.; Wang, Z. M.; Yang, X.; Ooi, K. *Langmuir* **2002**, *18*, 4926.
(50) Hassan, H. M. A.; Abdelsayed, V.; Khder, A. E. R. S.; AbouZeid, K. M.; Terner, J.; El-Shall, M. S.; Al-Resayes, S. I.; El-Azhary, A. A. *J. Mater. Chem.* **2009**, *19*, 3832.
(51) McAllister, M. J.; Li, J. L.; Adamson, D. H.; Schniepp, H. C.; Abdala, A. A.; Liu, J.; Herrera-Alonso, M.; Milius, D. L.; Car, R.; Prud'homme, R. K.; Aksay, I. A. *Chem. Mater.* **2007**, *19*, 4396.
(52) Nethravathi, C.; Nisha, T.; Ravishankar, N.; Shivakumara, C.; Rajamathi, M. *Carbon* **2009**, *47*, 2054.
(53) Lambert, T. N.; Chavez, C. A.; Hernandez-Sanchez, B.; Lu, P.; Bell, N. S.; Ambrosini, A.; Friedman, T.; Boyle, T. J.; Wheeler, D. R.; Huber, D. L. *J. Phys. Chem. C* **2009**, *113*, 19812.
(54) Xu, C.; Wu, X.; Zhu, J.; Wang, X. *Carbon* **2008**, *46*, 386.
(55) Briggs, D, Beamson, G. *High Resolution XPS of Organic Polymers: The Scienta ESCA300 Database*; John Wiley and Sons: New York, 1992.
(56) Yan, X.; Chen, J.; Yang, J.; Xue, Q.; Miele, P. *ACS Appl. Mater. Interfaces* **2010**, *2*, 2521.
(57) Bronoel, G.; Millot, A.; Tassin, N. *J. Power Sources* **1991**, *34*, 243.
(58) Ferrari, A. C.; Robertson, J. *Phys. Rev. B* **2000**, *61*, 14095.
(59) Gómez-Navarro, C.; Weitz, R. T.; Bittner, A. M.; Scolari, M.; Mews, A.; Burghard, M.; Kern, K. *Nano Lett.* **2007**, *7*, 3499.
(60) Stankovich, S.; Dikin, D. A.; Piner, R. D.; Kohlhaas, K. A.; Kleinhammes, A.; Jia, Y.; Wu, Y.; Nguyen, S. T.; Ruoff, R. S. *Carbon* **2007**, *45*, 1558.
(61) Dreyer, D. R.; Park, S.; Bielawski, C. W.; Ruoff, R. S. *Chem. Soc. Rev.* **2010**, *39*, 228.
(62) Fan, X.; Peng, W.; Li, Y.; Li, X.; Wang, S.; Zhang, G.; Zhang, F. *Adv. Mater.* **2008**, *20*, 4490.
(63) Wu, Z. S.; Ren, W.; Wen, L.; Gao, L.; Zhao, J.; Chen, Z.; Zhou, G.; Li, F.; Cheng, H. M. *ACS Nano* **2010**, *4*, 3187.
(64) Xu, M. W.; Bao, S. J.; Li, H. L. *J. Solid State Electrochem.* **2007**, *11*, 372.
(65) Zhu, W. H.; Ke, J. J.; Yu, H. M.; Zhang, D. J. *J. Power Sources* **1995**, *56*, 75.
(66) Corrigan, D. A.; Bendert, R. M. *J. Electrochem. Soc.* **1989**, *136*, 723.
(67) Liu, X. M.; Zhang, Y. H.; Zhang, X. G.; Fu, S. Y. *Electrochim. Acta* **2004**, *49*, 3137–3141.
(68) Di Fabio, A.; Giorgi, A.; Mastragostino, M.; Soavi, F. *J. Electrochem. Soc.* **2001**, *148*, A845.